JPhys Photonics

PAPER · OPEN ACCESS

Characteristics of 1D ordered arrays of optical centers in solid-state photonics

To cite this article: Trevor Kling and Mahdi Hosseini 2023 J. Phys. Photonics 5 024003

View the article online for updates and enhancements.

You may also like

- Screening and engineering of colour centres in diamond
 Tobias Lühmann, Nicole Raatz, Roger John et al.
- Spectroscopic, dielectric properties and local structure observation by EXAFS for Nd,Y:CaF₂ crystal F K Ma, Q Zhang, D P Jiang et al.
- Spectroscopic and laser properties of Tm³⁺ optical centers in CaF₂ crystal under 795 nm diode laser excitation M E Doroshenko, O K Alimov, A G Papashvili et al.

Journal of Physics: Photonics



OPEN ACCESS

RECEIVED

9 February 2023

REVISED

3 April 2023

ACCEPTED FOR PUBLICATION

13 April 2023

PUBLISHED

2 May 2023

Original Content from this work may be used under the terms of the Creative Commons Attribution 4.0 licence.

Any further distribution of this work must maintain attribution to the author(s) and the title of the work, journal citation and DOI.



PAPER

Characteristics of 1D ordered arrays of optical centers in solid-state photonics

Trevor Kling^{1,2,*} and Mahdi Hosseini^{1,2}

- Birck Nanotechnology Center and Purdue Quantum Science and Engineering Institute, Elmore Family School of Electrical and Computer Engineering, Purdue University, West Lafayette, IN 47907, United States of America
- Department of Physics and Astronomy, Purdue University, West Lafayette, IN 47907, United States of America
- * Author to whom any correspondence should be addressed.

E-mail: klingt@purdue.edu

Keywords: quantum optics, solid state, cavity QED

Abstract

Collective interaction of emitter arrays has lately attracted significant attention due to its role in controlling directionality of radiation, spontaneous emission and coherence. We focus on light interactions with engineered arrays of solid-state emitters in photonic resonators. We theoretically study light interaction with an array of emitters or optical centers embedded inside a microring resonator and discuss its application in the context of solid-state photonic systems. We discuss how such arrays can be experimentally realized and how the inhomogeneous broadening of mesoscopic atomic arrays can be leveraged to study broadband collective excitations in the array.

1. Introduction

Coherent interaction of light with an ensemble of atoms is actively pursued for implementation of quantum optical platforms to generate, store and process quantum optical information. The strength of interaction between light and atoms is key to efficient and deterministic control of quantum information. As an example, distribution of quantum optical entanglement can be done more efficiently, in principle, when photonic qubits interact strongly with single atoms [1] compared to weak interaction with many atoms [2]. A conventional approach to increasing the light-atom interaction is to use low-loss and small-mode-volume optical resonators built around the atoms or optical centers [3].

In solids, an ensemble of atoms exhibits inhomogeneous broadening due to defects in the host material. High-bandwidth interaction has been achieved in small doped crystals with this property [4]. Using optical resonators to reach the strong-coupling regime, in this case, limits the interaction bandwidth due to the resonator linewidth. Therefore, exploring interaction mechanisms that enable strong light-atom coupling over a wide range of frequencies is desirable to advance quantum photonic technology and achieve broadband control of quantum optical information.

It has been proposed that an array of 2D or 3D identical atoms (or emitters) forming a periodic structure in space can coherently interact with light [5, 6] as an atomic mirror or they can superradiantly emit photons in certain directions. In 1D, laser-cooled atoms placed near a waveguide have also been shown to reach the strong coupling regime [7]. In these scenarios, atoms are considered to be identical (e.g. laser cooled atoms) and that imposes limitations on system's bandwidth (MHz) and its practical realization, which is due to the complex experimental setup required for laser trapping atoms. In this paper, we consider a mesoscopic 1D array of solid-state atoms coherently and collectively interacting with light over a wide range of frequencies. We discuss how such arrays can be implemented in solid-state photonics with large atom numbers and arbitrary geometries. Primarily, we present the theory to analyze the emission properties of such arrays and discuss its applications.

2. Physical system and experimental realization

The rare-earth ions in bulk crystals have been used to demonstrate broadband quantum light storage and these systems have the potential to reach coherence time on the order of hours [8]. Rare earth ions randomly

Figure 1. (a) An standing-wave pump was used to create (via the holeburning process) an effective array in a randomly Er-doped Y_2SiO_5 (YSO) crystal [13]. The effective array could then create an atomic Bragg grating reflecting the probe light after the holeburning process was completed.(b) An array of Er ions was precisely implanted into a SiN microring resonator. Enhanced light collection (reduced loss) was observed at a wavelength commensurate with the lattice [14]. (c) An array of Tm ions implanted into a lithium niobate microring resonator can exhibit long-range coupling with superradiance signatures [13].

doped in a miniaturized optical resonator have also been used to show strong light-atom interactions over the resonator linewidth [9, 10].

Recently, our group has investigated interactions of photons with 1D arrays of rare-earth ions in solid-state crystals and photonic structures. In one experiment (see figure 1(a)), we used a randomly doped Er crystal to engineer an effective array inside the crystal [11]. We created the array by means of spatio-temporal hole burning to tailor an atomic profile with a periodic spatial distribution in one dimension. We showed that this effective array can behave like an atomic mirror coherently reflecting light ($E_{\rm ref}$) in the same direction as the input light ($E_{\rm input}$).

In another experiment, we used precision ion implantation to deterministically create a periodic array of isotopically-pure Er ions inside a SiN microring resonator (see figure 1(b)). Microring resonators have been proposed as a scalable platform for light-atom interactions in solid-state systems [12]. We showed that in this platform, coherent interference between the scattered light inside the microring can be manifested as the reduced propagation loss at wavelengths commensurate with the array. Due to the amorphous structure of the SiN host, the inhomogeneous broadening and the decoherence rate of Er ions were large in this platform preventing us from observing of quantum interference or strong interactions.

To reach the quantum regime of light interaction with an ensemble of rare-earth ions, we also carried out experiments with an array of isotopically pure Tm^{3+} ions implanted inside a lithium niobate (LN) microresonator (see figure 1(c)). The crystalline structure of LN shows lower inhomogeneous broadening and decoherence for Tm^{3+} ions compared to Er^{3+} ions in SiN. Also, the large branching ratio of Tm^{3+} compared to Er^{3+} at the measured transition makes it easier to observe the collective decay effects. We were able to observe superradiance emission of photons from Tm^{3+} ions in LN resonators. The superradiance is the evidence of strong coupling of an array of solid-state optical centers with light. We note that the microresonator used in this study had large linewidth, and as the result a strong coupling could not be obtained by using the resonator alone. The geometry of ions enables interference between the light scattered by the ions, leading to directional and nonlinear emission. The emission between individual ions and its interference can be modeled as an effective coupling field between the ions that leads to long-range ion-ion coupling. The large inhomogeneous broadening of implanted ions and the relatively large cavity linewidth enables observation of collective light-atom coupling over a wide range of frequencies.

Typical microring resonators fabricated for photonic devices in LN have radii on the order of tens to hundreds of micrometers. These rings have a wide transmission window such that the intracavity fields can interface with Thulium or Erbium ions respectively. For our application, we fabricate rings with radius $R \approx 100~\mu m$ as shown in figure 2. The width of these waveguides is chosen to be sufficiently small to isolate the fundamental TE mode. The surface roughness of the ring dominates the scattering loss, modeled by a decay rate κ . Current state-of-the-art fabrication can produce rings with decay rates on the order of megahertz [15]. The ring is coupled to the rest of the optical elements via a bus waveguide, carrying driving fields E_1 and E_2 .

Into this microring, we have previously implanted Tm^{3+} ions in bands approximately 36 nanometers in width. The 3H_6 to 3H_4 transition of these ions corresponds to the desired 795 nanometer light, with a branching ratio close to unity for isotopically pure Thulium ions [16]. As a result, these ions can be considered as two-level systems coupled to our optical resonator modes. We then capture the decay to non-cavity modes by these ions as another decay rate Γ_0 .

When emitters such as rare-earth ions are incorporated into solid-state nanostructures, they experience an inhomogeneous broadening of the transition frequencies on the order of gigahertz [16]. Understanding

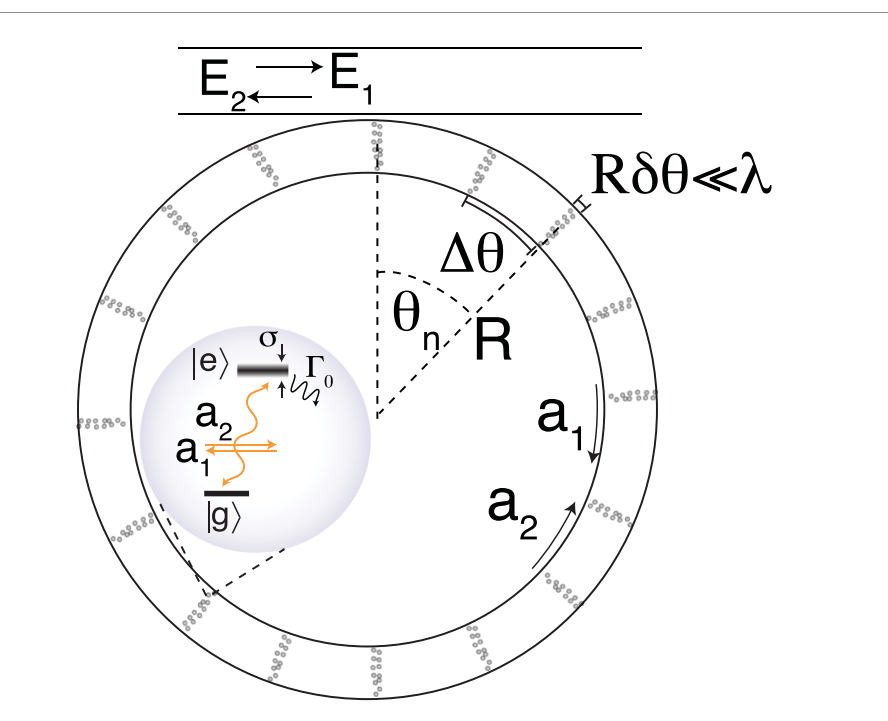


Figure 2. Schematic representation of the physical system under study. Atoms or optical centers are confined in segments much smaller than the optical wavelength around a microring resonator. The segments contain atoms of different frequencies and form an array around the resonator.

the role of inhomogeneous broadening in cooperative coupling is of great practical importance and, to the best of our knowledge, it has not been studied in details. In this paper, we provide a theoretical model for studying light-atom interaction in solid-state media with inhomogeneous broadening. We discuss the influence of this broadening on collective behaviors in 1D microring structures as defined above. We show that the interplay between atomic and cavity broadening enables broadband cooperative effects.

3. Theory for collective coupling in a ring resonator

Recently, there has been a great degree of interest in the effects of geometry on atomic ensembles coupled to a photonic medium. Atoms placed near a waveguide can induce an effective cavity mode, resulting in collective behaviors for atoms distributed in a lattice [17, 18]. Such systems have been used to engineer cooperatively enhanced atom-atom interactions [19] and coherent storage of photons in a lattice [20]. We consider an array of emitters inside a microring resonator coupled to counter-propagating modes. In the ring geometry considered, \hat{a}_1 and \hat{a}_2 denote the clockwise- and counterclockwise-propagating cavity modes, respectively. The atoms of uniform transition frequency ω_a are distributed within the waveguide and confined in segments of width much less than the wavelength (λ) , located at angles θ_n . The bare light-atom coupling strength is given by $g_0 = d\sqrt{\omega/2\hbar\varepsilon_0 A}$ for dipole matrix element d, cross-section A, and driving field frequency ω . It is assumed to be identical for all atoms. In general, the cavity linewidth is assumed to be much greater than the linewidth of an atom. Thus, we model the intracavity field as a broadband field equation with mode frequency $\omega_0(k)$ in analogy to [21]. Initially, we will consider the case of a system of unbroadened atoms. The Hamiltonian of the system is given in terms of the Fourier components of the intracavity field as

$$\begin{split} \hat{H} &= \int_{0}^{\infty} \mathrm{d}k \, \omega_{0}(k) \{ \hat{a}_{1}^{\dagger}(k,t) \hat{a}_{1}(k,t) + a_{2}^{\dagger}(k,t) a_{2}(k,t) \} + \frac{\omega_{a}}{2} \sum_{n=1}^{N} \hat{\sigma}_{z}^{(n)}(t) \\ &+ g_{0} \sum_{n=1}^{N} \hat{\sigma}_{eg}^{(n)} \int_{0}^{\infty} \mathrm{d}k \{ \hat{a}_{1}(k,t) e^{ikR\theta_{n}} + \hat{a}_{2}(k,t) e^{-ikR\theta_{n}} \} + g_{0} \sum_{n=1}^{N} \hat{\sigma}_{ge}^{(n)} \int_{0}^{\infty} \mathrm{d}k \{ \hat{a}_{1}^{\dagger}(k,t) e^{-ikR\theta_{n}} + \hat{a}_{2}^{\dagger}(k,t) e^{ikR\theta_{n}} \} \\ &+ \int_{0}^{\infty} \mathrm{d}k (E_{1}^{(in)}(k) \hat{a}_{1}(k,t) + E_{1}^{(in)*}(k) \hat{a}_{1}^{\dagger}(k,t)) + \int_{0}^{\infty} \mathrm{d}k (E_{2}^{(in)}(k) \hat{a}_{2}(k,t) + E_{2}^{(in)*}(k) \hat{a}_{2}^{\dagger}(k,t)). \end{split}$$
(1)

Here $\hat{\sigma}_z^{(i)}$ and $\hat{\sigma}_{ge}^{(i)}$ are the operators for the atomic population and coherence of ith segment, respectively. $E_i^{(in)}(k)$ denotes a classical driving field acting on the cavity mode k in direction j, and we assume that the

intracavity field has a linear mode dispersion $\omega_0(k) = \pm v_p k$ for uniform phase velocity v_p . We consider dissipation due to cavity decay at a rate κ and atomic decay to non-cavity modes at a rate Γ_0 ,

$$D(\hat{\rho}) = \frac{\Gamma_0}{2} \sum_{n=1}^{N} (2\hat{\sigma}_{ge}^{(n)} \hat{\rho} \hat{\sigma}_{eg}^{(n)} - \{\hat{\sigma}_{ee}^{(n)}, \hat{\rho}\})$$

$$+ \frac{\kappa}{2} \int_0^{\infty} dk (2\hat{a}_1(k, t) \hat{\rho} \hat{a}_1^{\dagger}(k, t) - \{\hat{a}_1(k, t)^{\dagger} \hat{a}_1(k, t), \hat{\rho}\})$$

$$+ \frac{\kappa}{2} \int_0^{\infty} dk (2\hat{a}_2(k, t) \hat{\rho} \hat{a}_2^{\dagger}(k, t) - \{\hat{a}_2(k, t)^{\dagger} \hat{a}_2(k, t), \hat{\rho}\}).$$
(2)

In its current form, equation (2) results in equations of motion of the atomic degrees of freedom containing field terms like

$$\frac{d}{dt}\hat{\sigma}_{ge}^{(n)}(t) = \left(-\Gamma_0 + i\omega_a\right)\hat{\sigma}_{ge}^{(n)} + ig_0\hat{\sigma}_z^{(n)} \int_0^\infty dk \left(\hat{a}_1(k,t)e^{ikR\theta_n} + \hat{a}_2(k,t)e^{-ikR\theta_n}\right). \tag{3}$$

The field-atom coupling in equation (3) contains the full expansion of the field terms. To eliminate these degrees of freedom, we define a field density operator $\hat{A}^{(sc)}(\theta,t)$ as

$$\hat{A}^{(sc)}(\theta,t) = \hat{A}_1(\theta,t) + \hat{A}_2(\theta,t) = \frac{1}{\sqrt{2\pi}} \int_0^\infty \hat{a}_1(k,t) e^{ikR\theta} dk + \frac{1}{\sqrt{2\pi}} \int_0^\infty \hat{a}_2(k,t) e^{-ikR\theta} dk. \tag{4}$$

To determine the equations for the field mode operators, we integrate the equations of motion of each operator with respect to time. The clockwise and counterclockwise field mode operators $\hat{a}_1(k,t)$ and $\hat{a}_2(k,t)$ have their dynamics given by

$$\frac{d}{dt}\hat{a}_{1}(k,t) = \left(-\frac{\kappa}{2} - i\omega_{0}(k)\right)\hat{a}_{1}(k,t) - ig_{0}\sum_{m=1}^{N}\hat{\sigma}_{ge}^{(m)}(t)e^{-ikR\theta_{m}} - iE_{1}^{(in)}(k)$$
(5)

$$\frac{d}{dt}\hat{a}_{2}(k,t) = \left(-\frac{\kappa}{2} - i\omega_{0}(k)\right)\hat{a}_{2}(k,t) - ig_{0}\sum_{m=1}^{N}\hat{\sigma}_{ge}^{(m)}(t)e^{ikR\theta_{m}} - iE_{2}^{(in)}(k). \tag{6}$$

The solutions to equations (5) and (6) are then given by

$$\hat{a}_{1}(k,t) = e^{(-\frac{\kappa}{2} - i\omega_{0}(k))t} \hat{a}_{1}(k,0) - ig_{0} \sum_{m=1}^{N} e^{-ikR\theta_{m}} \int_{0}^{t} \hat{\sigma}_{ge}^{(m)}(t') e^{(-\frac{\kappa}{2} - i\omega_{0}(k))(t-t')} dt' + \frac{iE_{1}^{(in)}(k)}{-\frac{\kappa}{2} - i\omega_{0}(k)}$$
(7)

$$\hat{a}_{2}(k,t) = e^{\left(-\frac{\kappa}{2} - i\omega_{0}(k)\right)t} \hat{a}_{2}(k,0) - ig_{0} \sum_{m=-1}^{N} e^{ikR\theta_{m}} \int_{0}^{t} \hat{\sigma}_{ge}^{(m)}(t') e^{\left(-\frac{\kappa}{2} - i\omega_{0}(k)\right)(t-t')} dt' + \frac{iE_{2}^{(in)}(k)}{-\frac{\kappa}{2} - i\omega_{0}(k)}.$$
(8)

To simplify, we define $\hat{A}_1^{(in)}(\theta) \equiv \int_0^\infty e^{ikR\theta} \hat{a}_1(k,0) dk$ and $\mathcal{E}_1(\theta) = \frac{i}{\sqrt{2\pi}} \int_0^\infty \frac{E^{(in)}(k)e^{ikR\theta}}{-\frac{\kappa}{2} - i\nu_p k} dk$. Performing the inverse Fourier transforms on equations (7) and (8) yields

$$\hat{A}_{1}(\theta,t) = e^{-\frac{\kappa}{2}t} \hat{A}_{1}^{(in)} \left(\theta - \frac{\nu_{p}}{R}t\right) - \frac{ig_{0}\sqrt{2\pi}}{\nu_{p}} \sum_{m=1}^{N} \int_{0}^{t} dt' \hat{\sigma}_{ge}^{(m)}(t') e^{-\frac{\kappa}{2}(t-t')} \delta\left(t' + \frac{R}{\nu_{p}}(\theta - \theta_{m}) - t\right) + \mathcal{E}_{1}(\theta).$$
(9)

Resolving the time-integral component of equation (9), we find a pair of step-functions due to the cyclical nature of the ring resonator.

$$\hat{A}_{1}(\theta,t) = e^{-\frac{\kappa}{2}t}\hat{A}_{1}^{(in)}\left(\theta - \frac{\nu_{p}}{R}t\right) + \mathcal{E}_{1}(\theta) - \frac{i\sqrt{2\pi}g_{0}}{\nu_{p}}\sum_{m=1}^{N}\left(\Theta(\theta - \theta_{m})e^{-\frac{\kappa}{2}\frac{R}{\nu_{p}}(\theta - \theta_{m})}\hat{\sigma}_{ge}^{(m)}\left(t - \frac{R}{\nu_{p}}(\theta - \theta_{m})\right)\right) + \Theta(\theta_{m} - \theta)e^{-\frac{\kappa}{2}\frac{R}{\nu_{p}}(2\pi - (\theta_{m} - \theta))}\hat{\sigma}_{ge}^{(m)}\left(t - \frac{R}{\nu_{p}}(2\pi - (\theta_{m} - \theta))\right).$$

$$(10)$$

The counter-clockwise component \hat{A}_2 follows identically, with $\theta-\theta_m$ replaced by $\theta_m-\theta$ and $\hat{A}_1^{(in)}\left(\theta-\frac{v_p}{R}t\right)$ replaced by $\hat{A}_2^{(in)}(\theta+\frac{v_p}{R}t)$ in equation (10) due to the opposite direction of propagation. The

term $A_{1,2}^{(in)}$ describes the delayed initial cavity fields at a position θ , and the term $\mathcal{E}_{1,2}(\theta)$ describes the time-independent effect of the classical driving field at a position θ . The field equation can then be viewed as two parts; an input term which describes the behavior of the input fields in the cavity, and a scattered field from each of the atoms. We also observe that the average time a photon spends in the cavity is given by $2\pi Rq/v_p = 1/\kappa$. Applying the Markov approximation for the atomic degrees of freedom and adding the counterclockwise field component, we find

$$\hat{A}^{(sc)}(\theta,t) = e^{-\frac{\kappa}{2}t} \left(\hat{A}_{1}^{(in)} \left(\theta - \frac{\nu_{p}}{R} t \right) + \hat{A}_{2}^{(in)} \left(\theta + \frac{\nu_{p}}{R} t \right) \right) + \left(\mathcal{E}_{1}(\theta) + \mathcal{E}_{2}(\theta) \right)$$

$$- \frac{i\sqrt{2\pi}qg_{0}}{\nu_{p}} \sum_{m=1}^{N} \mathcal{N}(\omega_{a}) \left(e^{\left(-\frac{\kappa}{2} + i\omega_{m}\right) \frac{R}{\nu_{p}} |\theta - \theta_{m}|} + e^{\left(-\frac{\kappa}{2} + i\omega_{m}\right) \frac{R}{\nu_{p}} (2\pi - |\theta - \theta_{m}|)} \right) \hat{\sigma}_{ge}^{(m)}(t).$$

$$(11)$$

Here, we have defined $\mathcal{N}(\omega) \equiv \frac{1}{q} \sum_{p=0}^{q-1} e^{\left(-\frac{\kappa}{2} + i\omega\right) \frac{R}{v_p}(2\pi p)}$, interpreted as the cavity effect for a mode of frequency ω . The $\mathcal{N}(\omega)$ term contains both real and imaginary parts; this accounts for both the destructive and constructive interference from the photon traveling in the microring cavity, as well as the buildup of phase for photons off-resonance with the cavity. q represents the average number of revolutions a photon makes before decaying out of the cavity. Making a transformation to include $\mathcal{N}(\omega)$ allows us to limit θ to the range $[0,2\pi)$. The scattered field includes two terms as each atom scatters a field in both the clockwise and counterclockwise directions. To further simplify the equations, we will write the per-atom scattered field amplitude as

$$\Omega_{nm} = \mathcal{N}(\omega_a) \left(e^{\left(-\frac{\kappa}{2} + i\omega_a\right)\frac{R}{\nu_p}|\theta_n - \theta_m|} + e^{\left(-\frac{\kappa}{2} + i\omega_a\right)\frac{R}{\nu_p}(2\pi - |\theta_n - \theta_m|)} \right). \tag{12}$$

This term encapsulates the effect of the phase between atoms at positions θ_n and θ_m on the coupling via a mode of frequency ω_a . In the case where the resonator decay for a single revolution is negligible and the atomic frequency is sufficiently close to a cavity resonance, we can write

$$\Omega_{nm} \approx \mathcal{N}(\omega_a) \left(e^{i\omega_a \frac{R}{\nu_p} |\theta_n - \theta_m|} + e^{-i\omega_a \frac{R}{\nu_p} |\theta_n - \theta_m|} \right) = 2\mathcal{N}(\omega_a) \cos\left(\omega_a \frac{R}{\nu_p} (\theta_n - \theta_m)\right). \tag{13}$$

When viewing the interatomic coupling, it is useful to express our coupling strength in terms of the cavity-enhanced cooperativity $\eta = \frac{g_0^2}{\kappa R \Gamma_0}$. Grouping both the clockwise and counterclockwise initial fields into a single term $A^{(in)}(\theta,t)$, we can write the equations of motion for the atomic population as

$$\frac{d}{dt}\hat{\sigma}_{z}^{(n)} = \left(-\Gamma_{0} - 2\eta\Gamma_{0}\Re(\mathcal{N}(\omega_{a}))\right)(\hat{\sigma}_{z}^{(n)} + 1)$$

$$-\sqrt{2\pi}ig_{0}(\hat{\sigma}_{eg}^{(n)}(e^{-\frac{\kappa}{2}t}\hat{A}^{(in)}(\theta_{n}, t) + \mathcal{E}(\theta_{n})) - (e^{-\frac{\kappa}{2}t}\hat{A}^{(in)\dagger}(\theta_{n}, t) + \mathcal{E}^{*}(\theta_{n}))\hat{\sigma}_{ge}^{(n)})$$

$$-2\eta\Gamma_{0}\sum_{m\neq n}\left(\Omega_{nm}^{*}\hat{\sigma}_{eg}^{(n)}\hat{\sigma}_{ge}^{(m)} + \Omega_{nm}^{*}\hat{\sigma}_{eg}^{(m)}\hat{\sigma}_{ge}^{(n)}\right).$$
(14)

In equation (14), the first line denotes the free-space evolution of the atomic population due to cavity-amplified decay to free space and repumping. The amplification term depends strongly on the atomic frequency; as the atoms are detuned away from the cavity resonance, the real part of $\mathcal{N}(\omega)$ decays quickly in amplitude. The term in the second line is the result of initial population of the resonator at t=0. Note that the terms $\hat{A}^{(in)}$ are explicitly time-dependent as the initial wave packet is not necessarily resonant with the cavity, and does not produce a standing wave. For a long-time steady state approximation, one can drop these terms as they decay exponentially. The final term describes an effective coupling between atoms mediated by the cavity field. The equations for the atomic coherence follow a similar form,

$$\frac{d}{dt}\hat{\sigma}_{ge}^{(n)}(t) = \left(-\frac{\Gamma_0}{2} - \eta\Gamma_0\mathcal{N}(\omega_a) + i\omega_a\right)\hat{\sigma}_{ge}^{(n)}(t) + \sqrt{2\pi}ig_0(e^{-\frac{\kappa}{2}t}\hat{A}^{(in)}(\theta_n, t) + \mathcal{E}(\theta_n))\hat{\sigma}_z^{(n)}(t) + \eta\Gamma_0\hat{\sigma}_z^{(n)}\sum_{m\neq n}\Omega_{nm}\hat{\sigma}_{ge}^{(m)}(t).$$
(15)

The last term in equation (15) indicates an effect on the inter-atomic coherences that depends on the inversion of each atomic dipole. Note that this term vanishes for two atoms in the ground state. The second term functions like a source term for the inter-atomic coherences, and indicates that the long-time evolution of the system will experience a nonzero steady-state interatomic coherence as the steady-state population

increases. Each atom in this ensemble experiences a cavity-induced enhancement to its emission rate given by $2\eta\Gamma_0\Re(\mathcal{N}(\omega))$, as well as a frequency shift $\eta\Gamma_0\Im(\mathcal{N}(\omega))$.

To better understand the role of the various terms in this equation, consider the case of all N atoms at the cavity-resonant frequency ω_0 . This corresponds to $k_0R = \omega_0 \frac{R}{\nu_p}$ being an integer. Assuming that the atoms are placed such that each atom is located at an antinode of the field, then the phase component of the couplings are universally one. Assuming that the evolution time of the system is long relative to κ , then the constants simplify to

$$\mathcal{N}(\omega_0) = \frac{1}{q} \frac{e^{-\frac{\kappa}{2}(2\pi(q+1))\frac{R}{\nu_p}} - 1}{e^{-\frac{\kappa}{2}(2\pi)\frac{R}{\nu_p}} - 1} \approx 1$$
(16)

$$\Omega_{nm,0} = \mathcal{N}(\omega_0) \left(e^{-\frac{\kappa_c}{2} \frac{R}{\nu_p} |\theta_n - \theta_m|} + e^{-\frac{\kappa_c}{2} \frac{R}{\nu_p} (2\pi - |\theta_n - \theta_m|)} \right) \approx 2.$$
 (17)

In the resulting equations, we assume that the classical driving field is symmetric for all atoms; i.e. $\mathcal{E}(\theta_i)$ is identical for all θ_i . Under these assumptions, all atoms behave identically regardless of position θ_i in the steady state. Thus, one has the symmetric expectation value relations $\langle \hat{\sigma}_z^{(n)} \rangle = \langle \hat{\sigma}_z^{(1)} \rangle$, $\langle \hat{\sigma}_{ge}^{(n)} \rangle = \langle \hat{\sigma}_{ge}^{(1)} \rangle$. Under these conditions and considering $\langle \hat{\sigma}_z^{(1)} \rangle = -1$, the steady-state single-atom and atom-atom coherence can be written respectively as

$$\langle \hat{\sigma}_{ge}^{(1)} \rangle_{SS} = \frac{\sqrt{2\pi} i g_0 \mathscr{E}}{-\frac{\Gamma_0}{2} - \eta \Gamma_0 (2N - 1) + i\omega_0} \quad \& \quad \langle \hat{\sigma}_{eg}^{(1)} \hat{\sigma}_{ge}^{(2)} \rangle_{SS} = \frac{2\pi g_0^2 |\mathscr{E}|^2}{\left(\frac{\Gamma_0}{2} + \eta \Gamma_0 (2N - 1)\right)^2 + \omega_0^2}. \tag{18}$$

Note that the atomic decay rate, Γ_0 , is modified by a factor of $1+4N\eta$ due to the collective coupling enhancing the directional scattering into the cavity mode. The emission rate of the system then scales linearly with the number of participating atoms in a fully-cooperative array. This collectively enhanced emission is mediated by the intracavity field, and is maximized when the atoms are all located at antinodes. When this collective decay rate exceeds the original decay rate Γ_0 , the system becomes 'superradiant' [22]. Under these conditions, the field scattered by the surrounding ensemble of atoms induces directional scattering.

3.1. Correlation in emission from atomic arrays

To better understand the effect of the atomic geometry on the emissions from the ring resonator, we consider the correlations between field components. The second order-correlation function, $g^{(2)}(\tau)$ can be used to quantify the degree of directionality of emission from an array of emitters. We can write $g^{(2)}(\tau)$ for correlation between modes i and j observed at a position \mathbf{r}_0 in terms of the field operators as

$$g_{ij}^{(2)}(t,\tau) = \frac{\langle \hat{A}_{i}^{\dagger}(\mathbf{r}_{0},t)\hat{A}_{j}^{\dagger}(\mathbf{r}_{0},t+\tau)\hat{A}_{j}(\mathbf{r}_{0},t+\tau)\hat{A}_{i}(\mathbf{r}_{0},t)\rangle}{\langle \hat{A}_{i}^{\dagger}(\mathbf{r}_{0},t)\hat{A}_{i}(\mathbf{r}_{0},t)\rangle\langle \hat{A}_{j}^{\dagger}(\mathbf{r}_{0},t+\tau)\hat{A}_{j}(\mathbf{r}_{0},t+\tau)\rangle}.$$
(19)

Let t denote the time at which the system reaches steady-state evolution. We consider exclusively the scattered field, ignoring the cavity driving field. Using the same time-evolution of the field modes as described above, we arrive at a spin-operator representation of equation (19),

$$g_{ij}^{(2)}(\tau) = \frac{\sum_{m,m',p',p} \alpha_{m,i}^* \alpha_{m',j}^* \alpha_{p',j} \alpha_{p,i} \langle \sigma_{eg}^{(m)}(0) \sigma_{eg}^{(m')}(\tau) \sigma_{ge}^{(p')}(\tau) \sigma_{ge}^{(p)}(0) \rangle}{\left(\sum_{m,p} \alpha_{m,i}^* \alpha_{p,i} \langle \sigma_{eg}^{(m)}(0) \sigma_{ge}^{(p)}(0) \rangle\right) \left(\sum_{m',p'} \alpha_{m',j}^* \alpha_{p',j} \langle \sigma_{eg}^{(m')}(\tau) \sigma_{ge}^{(p')}(\tau) \rangle\right)}$$
(20)

where $\alpha_{m,i}$ denotes the coupling between an atom m and a field mode i. For the case of our ring resonator, this $\alpha_{m,i}$ contains both the coupling strength g and a position-dependent effect $e^{ik_aR(\theta-\theta_i)}$. For $\tau=0$, in the case of complete atomic inversion these expectation values have well-known forms:

$$\langle \sigma_{eg}^{(m)}(0)\sigma_{eg}^{(m')}(0)\sigma_{ge}^{(p')}(0)\sigma_{ge}^{(p)}(0)\rangle = (\delta_{mp}\delta_{m'p'} + \delta_{mp'}\delta_{m'p})(1 - \delta_{mm'})$$
(21)

$$\langle \sigma_{eg}^{(m)}(0)\sigma_{ge}^{(p)}(0)\rangle = \delta_{mp}. \tag{22}$$

For N unbroadened atoms at the resonant frequency of the cavity in a ring resonator with placements given by $\theta_1, \dots, \theta_N$, we find the following results for emissions into co- and counter-propagating modes the same frequency:

$$g_{11}^{(2)}(0) = \frac{1}{N^2} \Big(2N(N-1) \Big)$$
 (23)

$$g_{12}^{(2)}(0) = \frac{1}{N^2} \left(4 \sum_{m=1}^{N} \sum_{m'>m} \cos^2(k_a R(\theta_{m'} - \theta_m)) \right). \tag{24}$$

For any N > 1, the upper and lower bounds for $g^{(2)}(0)$ are given by

$$\frac{(N-2)}{N} \leqslant g_{12}^{(2)}(0) \leqslant \frac{(2N-2)}{N}.$$
 (25)

The maximum value of equation (24) is achieved when the interatomic spacing is $\lambda/2$, as then $R(\theta_{m'}-\theta_m)=n\lambda/2=n\pi/k_a$. In the special case of two atoms in a ring resonator, the $g^{(2)}$ function can be simplified as $g_{12}^{(2)}(0)=\cos^2(k_aR(\theta_m-\theta_{m'}))$. This case was recently studied experimentally for two defect centers in a SiC microdisk [6], and it was demonstrated that this system can allow for selection of only the copropagating modes by angular spacing of $\pi/2$. Note that the limits derived for the N-atom case implies that this effect is unique to the 2-atom regime. In the two-atom case, the atomic phase or position can be engineered such that perfect constructive or destructive interference between interactivity radiation fields can be observed. As the number of atoms increases, the atoms can no longer be positioned such that the interference between all atoms is completely destructive and one sees reduced emissions in the counterpropagating modes. The influence of geometry on the emergence of superradiant behavior has been previously evaluated in free space in [23, 24]. In the case of a resonator, the directionality of these bursts is replaced by a preference for a particular direction of propagation within the waveguide.

3.2. Effect of inhomogeneous broadening in atomic arrays

In the prior section, we developed a theory for handling atoms of any frequency coupled to a ring resonator. We now consider an ensemble of atoms with frequency distribution, e.g. inhomogeneous broadening in solids. We consider atoms at the desired frequency ω_a resonant with the optical mode, and the other atoms can be considered via an effective coupling between the modes of the field β . $M(\Delta)$ denotes the number of broadened atoms within each band at a detuning from the atomic resonance Δ . We denote the number of unbroadened atoms then as M_0 , and we assume that the density of atoms follows a Gaussian distribution $(\sqrt{2\pi}\sigma)^{-1} \exp(-\Delta^2/2\sigma^2)$ with standard deviation σ . These atoms have a detuning-dependent interaction with the field;

$$\hat{H}/\hbar = \int_{0}^{\infty} dk \left\{ \omega_{0}(k) (\hat{a}_{1}^{\dagger}(k,t) \hat{a}_{1}(k,t) + \hat{a}_{2}^{\dagger}(k,t) \hat{a}_{2}(k,t)) - \beta(k) \hat{a}_{1}^{\dagger}(k,t) \hat{a}_{2}(k,t) - \beta(k)^{*} \hat{a}_{2}^{\dagger}(k,t) \hat{a}_{1}(k,t) \right\}
+ \frac{\omega_{0}}{2} \sum_{m=1}^{M_{0}} \hat{\sigma}_{z}^{(m)} + g_{0} \sum_{m=1}^{M_{0}} \sigma_{eg}^{(m)} \int_{0}^{\infty} dk (\hat{a}_{1}(k,t) e^{ikR\theta_{m}} + \hat{a}_{2}(k,t) e^{-ikR\theta_{m}})
+ g_{0} \sum_{m=1}^{M_{0}} \sigma_{ge}^{(m)} \int_{0}^{\infty} dk (\hat{a}_{1}^{\dagger}(k,t) e^{-ikR\theta_{m}} + \hat{a}_{2}^{\dagger}(k,t) e^{ikR\theta_{m}})
+ \int_{0}^{\infty} dk (E_{1}^{(in)}(k) \hat{a}_{1}(k,t) + E_{1}^{(in)*}(k) \hat{a}_{1}^{\dagger}(k,t))
+ \int_{0}^{\infty} dk (E_{2}^{(in)}(k) \hat{a}_{2}(k,t) + E_{2}^{(in)*}(k) \hat{a}_{2}^{\dagger}(k,t)).$$
(26)

Here, all M_0 of the atoms have resonant frequency ω_a and the broadened atoms contribute to the term β . We consider a distribution of atoms consisting of B total bands inside the host material. Each band consists of an atomic ensemble localized in the host via, for example, focused ion implantation, and spacing between the bands can be controlled to form certain geometries of the entire ensemble. The simple geometry considered here is a periodic array of bands in 1D and along the field's propagation direction. The coefficient β can be determined by the power emitted into the counter-propagating mode normalized to the total power in a single field mode. We follow the same procedure for calculating this as [25]. Assuming atoms are contained within a 1D waveguide, there exist M inhomogeneously broadened atoms at ith band's position $\{\theta_i\}$ which are responsible for this scattering.

To construct the coefficient, we can write $|\beta|$ in terms of the emitted power,

$$|\beta(\omega)| = \frac{\omega}{2} \int_{-\infty}^{\infty} \frac{P_{4\pi}^{(0)}(\omega, \omega')}{P_{in}(\omega, \omega')} \frac{P_{cM}(\omega, \omega')}{P_{4\pi}^{(0)}(\omega, \omega')} d\omega'$$
(27)

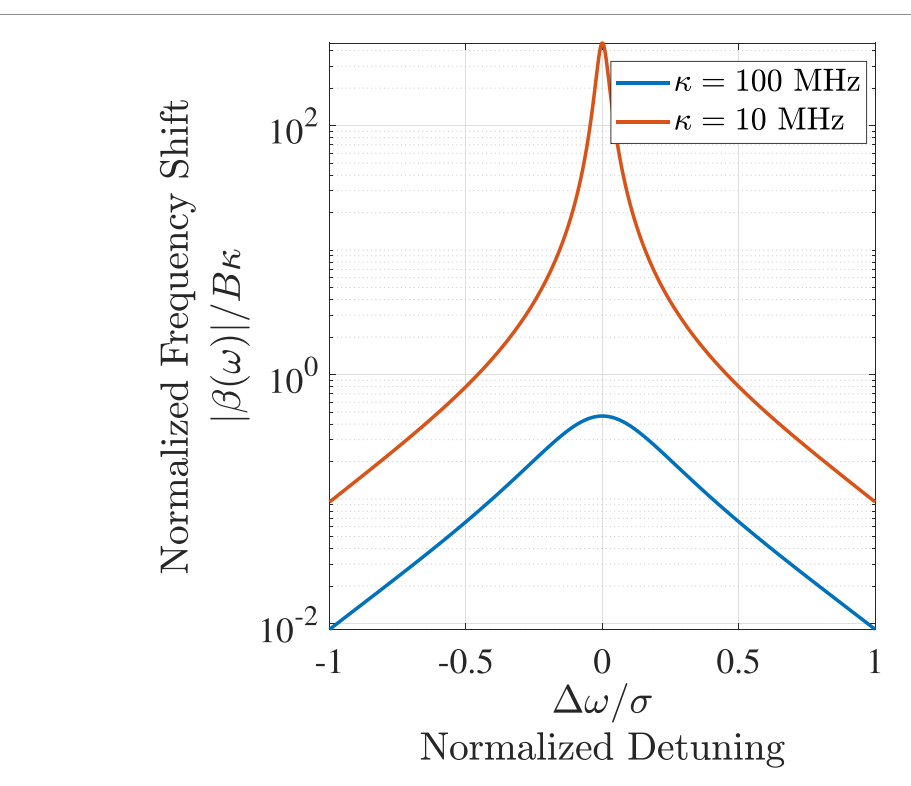


Figure 3. Coupling between modes with an incident field detuned from cavity resonance by $\Delta\omega$. Simulation parameters $\{N, \omega_a, v_p, R, \Gamma, g_0, \sigma\} = \{4 \times 10^6, 378\,\text{THz}, 3 \times 10^8\,\,\text{m s}^{-1}, 50\,\,\mu\text{m}, 1\,\text{KHz}, 10\,\text{KHz}, 0.42\,\text{GHz}\}$. The detuning is normalized to the standard deviation of the inhomogeneous broadening distribution, and the coupling strength is normalized by the cavity decay rate and number of implanted segments or bands.

where $P_{4\pi}^{(0)}$ is the power scattered by a single atom into free space in the absence of a cavity, P_{in} is the incoming power from the counter-propagating mode, and P_{cM} is the power scattered into the cavity mode by M atoms at a single frequency. These ratios can be found via similar method as [26], that in the rotating wave approximation yield

$$|\beta(\omega)| = \frac{\omega}{2} \int_{-\infty}^{\infty} \left(\frac{|H(\Delta)|^2 M(\Delta)^2 \eta^2 \mathcal{L}_a(\Delta)}{(1 + M(\Delta)H(\Delta)\eta \mathcal{L}_a(\Delta))^2 + (\frac{2\delta}{\kappa} + M(\Delta)H(\Delta)\eta \mathcal{L}_d(\Delta))^2} \right) d\Delta$$
(28)

where $\Delta = \omega - \omega_a$ is the detuning between the incident field and the broadened atoms, $\delta = \omega - \omega_c$ is the detuning between the incident field and the cavity resonance, $\mathcal{L}_a(\Delta) = \Gamma^2/(\Gamma^2 + 4\Delta^2)$ is defined as the absorptive lineshape, and $\mathcal{L}_d(\Delta) = -2\Gamma\Delta/(\Gamma^2 + 4\Delta^2)$ as the dissipative lineshape. $H(\Delta) = \sum_{n=1}^{B} \cos^2(\omega \frac{R}{v_p} \theta_n)$ denotes the response of an atomic dipole within the cavity for each band due to the field detuned from their resonance by Δ . An example of the resulting mode-mode coupling, β (normalized to B, the number of atomic bands, and κ , the cavity decay rate) as a function of the incident field frequency is shown in figure 3. The coupling takes the form of a Voigt profile, brought about by the Lorentzian absorption of individual atoms and the Gaussian distribution of frequencies.

To decouple field's equations, we define the standing-wave operators

$$\hat{a}_{SW,1} = \frac{1}{\sqrt{2}} (\hat{a}_1 + e^{i\phi} \hat{a}_2)$$

$$\hat{a}_{SW,2} = \frac{1}{\sqrt{2}} (\hat{a}_1 - e^{i\phi} \hat{a}_2)$$
(29)

where $\beta(\omega) = |\beta(\omega)|e^{i\phi(\omega)}$. For the following derivation, we will employ the linear dispersion to write β in terms of the wavevector k. The evolution of the new field is then given by the two uncoupled equations

$$\frac{d}{dt}\hat{a}_{SW,1}(k,t) = \left(-\frac{\kappa}{2} - i\omega_0(k) - i|\beta(k)|\right)\hat{a}_{SW,1}(k,t) - i\frac{g_0}{\sqrt{2}}\sum_{m=1}^{M_0} \left(e^{-ikR\theta_m} + e^{i(kR\theta_m + \phi(k))}\right)\hat{\sigma}_{ge}^{(m)}(t) - \frac{i}{\sqrt{2}}\left(E_1^{(in)}(k) + e^{i\phi(k)}E_2^{(in)}(k)\right) \tag{30}$$

$$\frac{d}{dt}\hat{a}_{SW,2}(k,t) = \left(-\frac{\kappa}{2} - i\omega_0(k) + i|\beta(k)|\right)\hat{a}_{SW,2}(k,t) - i\frac{g_0}{\sqrt{2}}\sum_{m=1}^{M_0} \left(e^{-ikR\theta_m} - e^{i(kR\theta_m + \phi(k))}\right)\hat{\sigma}_{ge}^{(m)}(t) - \frac{i}{\sqrt{2}}\left(E_1^{(in)}(k) - e^{i\phi(k)}E_2^{(in)}(k)\right).$$
(31)

Note that the subscripts no longer correspond to the direction of propagation for the fields, as both modes are hybridized by β . Instead, $\hat{a}_{SW,1}(k,t)$ corresponds to a field mode with positively-shifted frequency, while $\hat{a}_{SW,2}(k,t)$ corresponds to a mode with negatively-shifted frequency. We can similarly write the equations of motion for the atoms,

$$\frac{d}{dt}\hat{\sigma}_{z}^{(n)} = (-\Gamma_{0})(\hat{\sigma}_{z}^{(n)} + 1) - i\frac{g_{0}}{\sqrt{2}}\hat{\sigma}_{eg}^{(n)}\int_{0}^{\infty}dk\Big((\hat{a}_{SW,1} + \hat{a}_{SW,2})e^{ikR\theta_{n}} + (\hat{a}_{SW,1} - \hat{a}_{SW,2})e^{-i\phi(k) - ikR\theta_{n}}\Big) \\
+ i\frac{g_{0}}{\sqrt{2}}\hat{\sigma}_{ge}^{(n)}\int_{0}^{\infty}dk\Big((\hat{a}_{SW,1}^{\dagger} + \hat{a}_{SW,2}^{\dagger})e^{-ikR\theta_{n}} + (\hat{a}_{SW,1}^{\dagger} - \hat{a}_{SW,2}^{\dagger})e^{i\phi(k) + ikR\theta_{n}}\Big) \tag{32}$$

$$\frac{d}{dt}\hat{\sigma}_{ge}^{(n)} = (-\Gamma_0 + i\omega_0)\hat{\sigma}_{ge}^{(n)} + i\frac{g_0}{\sqrt{2}}\hat{\sigma}_z^{(n)}\int_0^\infty dk \Big((\hat{a}_{SW,1} + \hat{a}_{SW,2})e^{ikR\theta_n} + (\hat{a}_{SW,1} - \hat{a}_{SW,2})e^{-i\phi - ikR\theta_n}\Big). \tag{33}$$

Systems of this form for constant β have been studied at length in [25], for the case of scattering from the walls of a ring resonator. However, the scattering here is frequency-dependent as the detuning of the atoms influences both the scattering rate and the imprinted phase. We write the field density operators for this system in a similar fashion to the explicit case,

$$A_1(\theta, t) \equiv \frac{1}{\sqrt{2\pi}} \int_0^\infty \hat{a}_{SW,1}(k, t) e^{ikR\theta} dk + \frac{1}{\sqrt{2\pi}} \int_0^\infty \hat{a}_{SW,2}(k, t) e^{ikR\theta} dk$$
 (34)

$$A_{2}(\theta,t) \equiv \frac{1}{\sqrt{2\pi}} \int_{0}^{\infty} \hat{a}_{SW,1}(k,t) e^{-ikR\theta - i\phi(k)} dk - \frac{1}{\sqrt{2\pi}} \int_{0}^{\infty} \hat{a}_{SW,2}(k,t) e^{-ikR\theta - i\phi(k)} dk.$$
 (35)

We then integrate these fields in a way very similar to equation (5) through (10). However, the discussion is complicated somewhat by the inclusion of the frequency-dependent $|\beta(\omega)|$ term. Writing the solutions for equation (30) explicitly,

$$\hat{a}_{SW,1}(k,t) = e^{\left(-\frac{\kappa}{2} - i\omega_{0}(\kappa) - i|\beta(k)|\right)t} \hat{a}_{SW,1}(k,0) + \frac{i}{\sqrt{2}} \frac{\left(E_{1}^{(in)}(k) + e^{i\phi(k)}E_{2}^{(in)}(k)\right)}{-\frac{\kappa}{2} - i\omega_{0}(k) - i|\beta(k)|} - i \frac{g_{0}}{\sqrt{2}} \sum_{m=1}^{N} \int_{0}^{t} dt' \hat{\sigma}_{ge}^{(m)}(t') e^{\left(-\frac{\kappa}{2} - i\omega_{0}(k) - i|\beta(k)|\right)(t-t')} \left(e^{-ikR\theta_{m}} + e^{i\phi(k) + ikR\theta_{m}}\right).$$
(36)

Note that the solution for $\hat{a}_{SW,2}$ follows identically save for a sign flip of $|\beta(k)|$ and $e^{i\phi(k)}$. Using these explicit forms in equation (34), we find

$$\hat{A}_{1}(\theta,t) = e^{-\frac{\kappa}{2}t} A_{1}^{(in)}(\theta,t) + \overline{\mathcal{E}}_{1}^{(in)}(\theta)
- i \frac{g_{0}}{2\sqrt{\pi}} \sum_{m=1}^{N} \int_{0}^{t} dt' \hat{\sigma}_{ge}^{(m)}(t') e^{-\frac{\kappa}{2}(t-t')} \left(\int_{0}^{\infty} e^{(-i\nu_{p}k-i|\beta(k)|)(t-t')-ikR\theta_{m}+ikR\theta} dk \right)
- i \frac{g_{0}}{2\sqrt{\pi}} \sum_{m=1}^{N} \int_{0}^{t} dt' \hat{\sigma}_{ge}^{(m)}(t') e^{-\frac{\kappa}{2}(t-t')} \left(\int_{0}^{\infty} e^{(-i\nu_{p}k+i|\beta(k)|)(t-t')-ikR\theta_{m}+ikR\theta} dk \right)$$
(37)

where $\overline{\mathscr{E}}_1^{(in)}$ encapsulates the effect of the driving fields on the clockwise field density. We note that this term includes contributions from both the clockwise and counterclockwise driving fields when $|\beta(k)|$ is nonzero. Additionally, we have applied the rotating-wave approximation to drop the fast oscillating

2 *k* terms. Generally, we can writte this equation in terms of the two input fields and a scattered field component $\hat{S}_{\beta}(\theta, t)$

$$\hat{A}_1(\theta,t) = e^{-\frac{\kappa}{2}t} A_1^{(in)}(\theta,t) + \overline{\mathcal{E}}_1^{(in)}(\theta) + \hat{S}_{\beta}(\theta,t). \tag{38}$$

We wish to simplify the terms in equation (37) in the same was as equation (10); to proceed, we employ Parseval's Theorem

$$\int_{-\infty}^{\infty} \tilde{f}^*(k)\tilde{g}(k)dk = 2\pi \int_{-\infty}^{\infty} f^*(x)g(x)dx$$
(39)

with $\tilde{f}(k) = e^{\pm i|\beta(k)|(t-t')}$ and $\tilde{g}(k) = \Theta(k)e^{ik(R(\theta-\theta')-\nu_p(t-t'))}$. Notably, the transform of $\tilde{g}(k)$ is now a delta function, as desired.

$$f(x) = \int_{-\infty}^{\infty} e^{\pm i|\beta(k)|(t-t') + ikx} dk \qquad g(x) = \frac{1}{\nu_p} \delta\left(\frac{R}{\nu_p}(\theta - \theta') - (t - t') + \frac{x}{\nu_p}\right). \tag{40}$$

We subsequently reorder the integrals in equation (37), finding that the scattered fields can be written as

$$\hat{S}_{\beta}(\theta,t) = -i\frac{\sqrt{\pi}g_{0}}{\nu_{p}} \sum_{m=1}^{N} \left[\int_{-\infty}^{\infty} dx \left(\int_{0}^{t} dt' \delta \left(t' - \left(t - \frac{R}{\nu_{p}} (\theta - \theta_{m}) - \frac{x}{\nu_{p}} \right) \right) \right. \\
\left. \times \left(e^{-\frac{\kappa}{2}(t - t')} \hat{\sigma}_{ge}^{(m)}(t') \int_{-\infty}^{\infty} dk e^{-i|\beta(k)|(t - t') - ikx} \right) \right) \\
+ \int_{-\infty}^{\infty} dx \left(\int_{0}^{t} dt' \delta \left(t' - \left(t - \frac{R}{\nu_{p}} (\theta - \theta_{m}) - \frac{x}{\nu_{p}} \right) \right) \right. \\
\left. \times \left(e^{-\frac{\kappa}{2}(t - t')} \hat{\sigma}_{ge}^{(m)}(t') \int_{-\infty}^{\infty} dk e^{i|\beta(k)|(t - t') - ikx} \right) \right].$$

$$(41)$$

Integrating equation (41) with respect to time places limits on the value of x, $-R(\theta - \theta_m) < x < v_p t$ $-R(\theta - \theta_m)$, as x values outside these bounds cannot have a nonzero value for the delta function.

$$\hat{S}_{\beta}(\theta,t) = -i\frac{\sqrt{\pi}g_{0}}{\nu_{p}} \sum_{m=1}^{N} \left[\int_{-R(\theta-\theta_{m})}^{\nu_{p}t-R(\theta-\theta_{m})} dx \left(e^{-\frac{\kappa}{2} \left(\frac{R}{\nu_{p}} (\theta-\theta_{m}) + \frac{x}{\nu_{p}} \right)} \hat{\sigma}_{ge}^{(m)} \left(t - \frac{R}{\nu_{p}} (\theta-\theta_{m}) - \frac{x}{\nu_{p}} \right) \right. \\
\left. \times \int_{-\infty}^{\infty} dk e^{-i|\beta(\omega)| \left(\frac{R}{\nu_{p}} (\theta-\theta_{m}) + \frac{x}{\nu_{p}} \right) - ikx} \right) \\
+ \int_{-R(\theta-\theta_{m})}^{\nu_{p}t-R(\theta-\theta_{m})} dx \left(e^{-\frac{\kappa}{2} \left(\frac{R}{\nu_{p}} (\theta-\theta_{m}) + \frac{x}{\nu_{p}} \right)} \hat{\sigma}_{ge}^{(m)} \left(t - \frac{R}{\nu_{p}} (\theta-\theta_{m}) - \frac{x}{\nu_{p}} \right) \right. \\
\left. \times \int_{-\infty}^{\infty} dk e^{i|\beta(\omega)| \left(\frac{R}{\nu_{p}} (\theta-\theta_{m}) + \frac{x}{\nu_{p}} \right) - ikx} \right) \right]. \tag{42}$$

Applying the Markov approximation to the atomic operators in equation (42), we can also reorder the equation to integrate the dummy variable x,

$$\hat{S}_{\beta}(\theta,t) = -i\frac{\sqrt{\pi}g_{0}}{\nu_{p}} \sum_{m=1}^{N} \left[\hat{\sigma}_{ge}^{(m)}(t)e^{\left(-\frac{\kappa}{2}+i\omega_{a}\right)\frac{R}{\nu_{p}}(\theta-\theta_{m})} \times \left(\int_{-\infty}^{\infty} dk e^{-i|\beta(k)|\frac{R}{\nu_{p}}(\theta-\theta_{m})} \int_{-R(\theta-\theta_{m})}^{\nu_{p}t-R(\theta-\theta_{m})} dx e^{\left(-\frac{\kappa}{2}+i\omega_{a}-i\nu_{p}k-i|\beta(k)|\right)\frac{x}{\nu_{p}}} \right) + \hat{\sigma}_{ge}^{(m)}(t)e^{\left(-\frac{\kappa}{2}+i\omega_{a}\right)\frac{R}{\nu_{p}}(\theta-\theta_{m})} \left(\int_{-\infty}^{\infty} dk e^{i|\beta(k)|\frac{R}{\nu_{p}}(\theta-\theta_{m})} \times \int_{-R(\theta-\theta_{m})}^{\nu_{p}t-R(\theta-\theta_{m})} dx e^{\left(-\frac{\kappa}{2}+i\omega_{a}-i\nu_{p}k+i|\beta(k)|\right)\frac{x}{\nu_{p}}} \right) \right].$$

$$(43)$$

Integrating and simplifying equation (43), we arrive at our final field equations

$$\hat{A}_{1}(\theta,t) = e^{-\frac{\kappa}{2}t} A_{1}^{(in)}(\theta,t) + \overline{\mathcal{E}}_{1}^{(in)}(\theta)
- i g_{0} \frac{\sqrt{\pi}}{v_{p}} \sum_{m=1}^{M_{0}} \left[\hat{\sigma}_{ge}^{(m)}(t) \int_{-\infty}^{\infty} d\omega \left(\tilde{\mathcal{N}}(\omega) e^{i\omega \frac{R}{v_{p}}(\theta - \theta_{m})} \right)
\times \left(\frac{e^{(-\frac{\kappa}{2} + i(\omega_{a} - \omega - |\beta(\omega)|))t} - 1}{-\frac{\kappa}{2} + i(\omega_{a} - \omega + |\beta(\omega)|)} + \frac{e^{(-\frac{\kappa}{2} + i(\omega_{a} - \omega + |\beta(\omega)|))t} - 1}{-\frac{\kappa}{2} + i(\omega_{a} - \omega + |\beta(\omega)|)} \right].$$
(44)

$$\hat{A}_{2}(\theta,t) = e^{-\frac{\kappa}{2}t} A_{2}^{(in)}(\theta,t) + \overline{\mathscr{E}}_{2}^{(in)}(\theta)
- ig_{0} \frac{\sqrt{\pi}}{\nu_{p}} \sum_{m=1}^{M_{0}} \left[\hat{\sigma}_{ge}^{(m)}(t) \int_{-\infty}^{\infty} d\omega \left(\tilde{\mathscr{N}}(\omega) e^{-i\omega \frac{R}{\nu_{p}}(\theta-\theta_{m})} \right)
\times \left(\frac{e^{(-\frac{\kappa}{2}+i(\omega_{a}-\omega-|\beta(\omega)|))t} - 1}{-\frac{\kappa}{2}+i(\omega_{a}-\omega-|\beta(\omega)|)} + \frac{e^{(-\frac{\kappa}{2}+i(\omega_{a}-\omega+|\beta(\omega)|))t} - 1}{-\frac{\kappa}{2}+i(\omega_{a}-\omega+|\beta(\omega)|)} \right) \right].$$
(45)

We have defined a phase factor $\tilde{\mathcal{N}}(\omega) = \sum_{p=0}^{q-1} e^{i\omega\frac{2\pi pR}{v_p}}$. In the limit as β goes to zero, we recover the original field equation by employing Fourier transform identities. Therefore, the effect of the inhomogeneous broadening can be understood by investigating the behavior and impacts of the integral parameter in these field equations. The effect is separable into a spatial component, independent of β or t, and a temporal component which depends on $|\beta|$. This effect also only depends on the detuning between the resonant atomic frequency and the broadening-induced resonance shift, $\Delta_{\beta} = (\omega_a - |\beta(\omega)|) - \omega$. This effect is purely real in the case that the atoms are on-resonance with the shifted cavity frequency, and is proportional to the cavity decay for a time t.

Note that the phase shift due to the inhomogeneous broadening $\phi(\omega)$ does not appear in either of these terms. This is due to the rotating wave approximation; the term $\phi(\omega)$ only appears in terms on the order of 2k or -2k. If we assume $\phi(\omega)$ is slowly oscillating relative to these terms, then it averages to zero.

One can subsequently write the field equations in terms of an effective spin-exchange rate and decay rate into the cavity, similarly to the formulation used in [27, 28]. We consider the long-time solution, where t is sufficiently large that the decaying exponentials can be ignored. In this scenario,

$$J_1^{nm}(\omega) = -g_0^2 \frac{(\omega_a - \omega - |\beta(\omega)|)}{\kappa^2 / 4 + (\omega_a - \omega - |\beta(\omega)|)^2} \left(\sum_{p=1}^{q-1} \exp\left(i\omega \frac{R}{\nu_p} (2\pi p + \theta_n - \theta_m)\right) \right)$$
(46)

$$\Gamma_1^{nm}(\omega) = g_0^2 \frac{\kappa}{\kappa^2 / 4 + (\omega_a - \omega - |\beta(\omega)|)^2} \left(\sum_{p=1}^{q-1} \exp\left(i\omega \frac{R}{\nu_p} (2\pi p + \theta_n - \theta_m)\right) \right)$$
(47)

where J_1^{nm} is the spin-exchange rate in the long-time limit for atoms n and m mediated by one of the standing waves, and Γ_1^{nm} is the corresponding decay rate. The integrand terms of equations (44) and (45) can be reinterpreted under these observations as the Fourier components of the total coupling between atoms n and m.

$$g(\omega, \theta_n, \theta_m) = \frac{J_1^{nm}(\omega) + J_2^{nm}(\omega)}{2} + i \frac{\Gamma_1^{nm}(\omega) + \Gamma_2^{nm}(\omega)}{4}.$$
 (48)

These Fourier components of the coupling are shown in figure 4 for a variety of interatomic spacings and cavity decay rates. The values are normalized to the maximum resonant coupling for unbroadened atoms in a cavity as seen in equation (10), $\eta\Gamma_0$. The effect of broadening-induced mode-mode coupling, β , is more pronounced for high-Q resonators where cavity decay rate is small compared to the width of the inhomogeneous broadening. For moderate optical Q factors, the atom-atom coupling can be observed in presence of broadening. In this regime, a change in lattice spacing, $R\Delta\theta$, can be seen as shift in atom-atom resonance. The results indicate that in the regime where single-atom cooperativity is small, the array can exhibit atom-atom enhanced coupling over a relatively wide range of frequencies.

Note that when the detuning between the probe field and the cavity resonance becomes zero, the coupling becomes purely imaginary. In this scenario, the inhomogeneous scattering does not contribute to spin-exchange interactions and instead simply suppresses the magnitude of the dissipative coupling. However, as Δ is shifted away from zero, $|\beta|$ contributes to suppressing this change in one of the Lorentzian

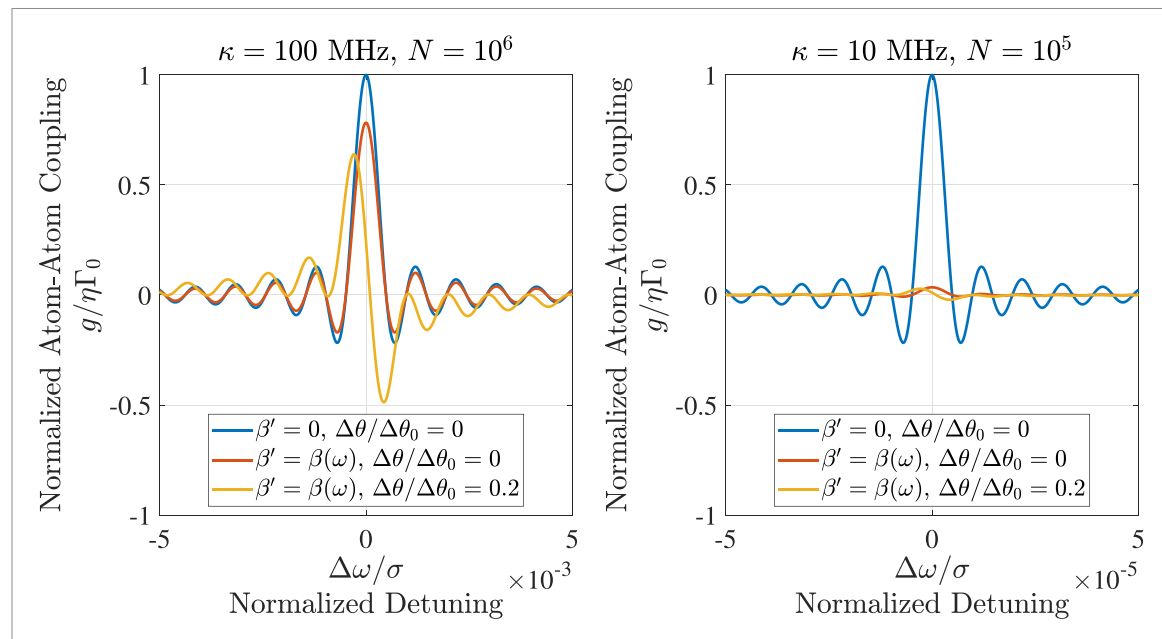


Figure 4. Coupling strength between atoms as a function of the field frequency ω , normalized to the unbroadened resonant cavity-enhanced atom-atom coupling. The blue lines represent the coupling at varying probe frequency for a system with no scattering due to inhomogeneous broadening, while the red and yellow lines denote the scattering-suppressed coupling at varying segment spacing. Simulation parameters $\{\omega_a, v_p, R, \Gamma, g_0, \sigma\} = \{378\,\text{THz}, 3 \times 10^8\,\text{m s}^{-1}, 50\,\mu\text{m}, 1\,\text{KHz}, 10\,\text{KHz}, 0.42\,\text{GHz}\}$. The spacing between the atoms $\Delta\theta$ being varied results in a shift in the optimal coupling frequency, and $\Delta\theta_0 = \lambda/R$ denotes the natural spatial period of the system. β' indicates the effect of inhomogeneous broadening considered for the simulation.

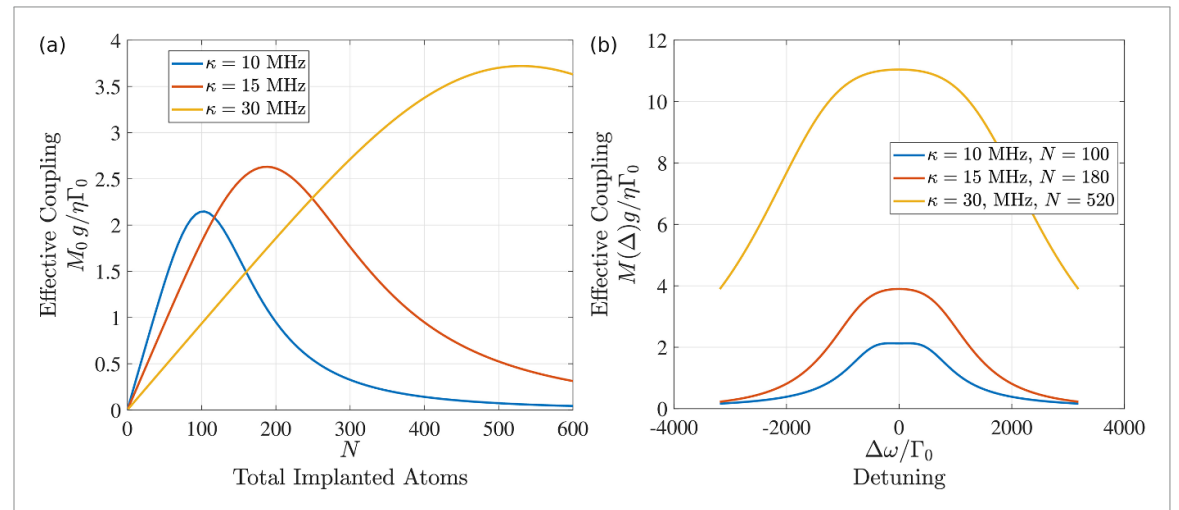


Figure 5. (a) Enhancement coupling coefficient as a function of number of implanted ions with inhomogeneous broadening. The system shows an initially linear improvement in coupling strength, before the suppression due to inhomogeneous broadening overcomes the linear amplification from an increasing atom number. Simulation parameters $\{\omega_a, v_p, R, \Gamma_0, g_0, \sigma\} = \{378\,\mathrm{THz}, 3\times10^8\,\mathrm{m\,s^{-1}}, 50\,\mu\mathrm{m}, 1\,\mathrm{KHz}, 10\,\mathrm{KHz}, 0.42\,\mathrm{GHz}\}$. The spacing between segments is taken to be $\lambda/2$, such that the collective behavior is maximized. (b) Enhancement to the collective coupling versus frequency for the ensemble. The system displays broadband enhancements to coupling due to the inhomogeneously broadened atoms. Each system is plotted with the optimal number of implanted ions, derived from plot (a). Simulation parameters $\{v_p, R, \Gamma_0, g_0, \sigma\} = \{3\times10^8\,\mathrm{m\,s^{-1}}, 50\,\mu\mathrm{m}, 1\,\mathrm{KHz}, 10\,\mathrm{KHz}, 0.42\,\mathrm{GHz}\}$. The detuning is taken relative to the unbroadened atomic frequency, $\omega_a = 378\,\mathrm{THz}$.

and enhances it in the other. In total, this coupling experiences a suppression of the amplitude of the Fourier components as a result of the inhomogeneous broadening.

Under these conditions, the suppression of the coupling strength depends on the number of atoms and broadening of the system. As a result, the scaling behavior of the coupling strength is not fully commensurate with increasing the number of atoms; instead, there exists some optimal number of atoms beyond which the loss in coupling strength due to scattering from broadened atoms exceeds the improvement in coupling due to additional resonant atoms. Figure 5(a) shows the enhancement in effective collective coupling for a variety of decay rates. $|\beta(\omega)|$ depends strongly on the cavity decay rate κ , with lower decay rates having much greater collective reflections. The inhomogeneously broadened atoms in these conditions can be interpreted as weakly-reflecting mirrors placed at the same location as the atoms modeled by the spin operators. As a

result, a geometry designed to optimize the atom-atom coupling will also maximize the backscattering from these weak mirrors.

We observe in figure 5(a) that the optimal coupling strength improves as κ increases. From equation (18), it is known that the decay rate of the system depends linearly on the effective coupling strength. This suggests that the superradiant character of the ensemble increases as the cavity confinement becomes worse, so long as a sufficient number of atoms are implanted. This superradiant effect can be interpreted as the initial linear improvement in effective coupling; the length of this linear region depends on the choice of cavity decay rate. However, while larger κ allows for the system to remain in this linear-scaling regime for larger numbers of atoms, it also reduces the magnitude of the coupling for equivalent numbers of atoms. In the limiting case of no cavity confinement, the system will see a linear improvement in coupling as expected for superradiant ensembles, but the magnitude of the coupling will be much smaller due to the lack of a cavity enhancement. We note that the current formulation of these terms does not factor in the dipole-induced dephasing for large ensembles; this results in a competing effect which will additionally suppress the collective behavior for high-density ensembles.

Figure 5(b) shows the coupling enhancement for atoms of varying frequency. Here the atomic frequency ω_a is allowed to vary, accounting for different subsets of the inhomogeneously broadened distribution. The system experiences enhanced coupling for detunings far outside the resonant atomic linewidth, which is increasingly broadband for greater cavity linewidths. Thus, these enhancements also correspond to a degree of broadband, long-range superradiance.

4. Discussion and applications

Superradiance for a localized ensemble of emitters in solids has been observed [29, 30]. When cooperative emission can occur, the inhomogeneous broadening in solids typically results in co-existence of sub- and super-radiance radiations [31]. When atoms with large inhomogeneous broadening form an ordered array, resonant excitation of the array enables the selection of a subclass of atoms with narrow resonant frequency distribution.

As discussed in the first section, an arbitrary large array of rare-earth ions can be created inside a solid-state photonic cavity. Although the single-atom coupling rate, g_0 , for most rare-earth ions is weak, by creating an array of ion segments where each segment contains a localized ensemble of n ions at the excitation frequency, the effective light-to-atomic-segment coupling rate can increase to $g\sqrt{n}$ due to the collective coupling effect. This is the case when off-resonant coupling is ignored. In a ring resonator geometry, long-range coupling between ions can be achieved due to the effective spin-spin coupling mediated by the cavity field. The rare-earth ions such as Er or Tm have excited state linewidth in the range of $\Gamma_0 = 1 - 100$ kHz. Assuming an inhomogeneous broadening of $\Delta\omega_{in} = 10$ GHz, a photonic cavity with linewidth of $\kappa = 1$ GHz can accommodate on the order of million excitation modes. At each excitation mode, a small fraction ($\sim 10^{-5}$) of atoms resonantly interact with the cavity mode. Assuming an implantation fluence of 10^{16} ions cm⁻², approximately 10^6 atoms can be implanted in each band or segment. For a resonator of circumference about 5 mm, a total of about 10^4 bands or segments can be created inside a resonator with $\lambda/2n_{\rm ref}$ spacing, where $n_{\rm ref}$ is the effective refractive index (considering $\lambda = 800$ nm). Considering these parameters, the optimum atom number for atom-atom coupling, as shown in figure 5, is within reach.

One application of cooperative emission in rare-earth solids can be in implementing superradiant lasers. Conventional lasers have limitations towards narrow emission spectra linewidth. Recently, superradiant lasing has been observed in cold alkaline earth atoms based on narrow linewidth of dipole-forbidden optical transitions [32]. Lasing linewidth on the order of kHz has been achieved [32]. It was shown that in this regime, sensitivity of laser frequency to fluctuations of the cavity length can be reduced by an order of magnitude [32]. As these experiments were carried out using laser-cooled atoms, the continuous repumping requirement to achieve continuous lasing causes heating of atoms due to the free-space scattering. In this scenario, the heating and atomic motion eventually suppresses lasing.

To implement on-chip lasers, rare-earth solids are being considered for this purpose. In a recent experiment, a microdisk resonator was fabricated on ytterbium-doped lithium niobate [33] on insulators, which has achieved lasing with conversion efficiency of 1.36%. In many cases, the lasing efficiency of rare-earth materials is limited by low atomic density and nonlinear effects at higher optical pump powers. The cooperative effects as described in this paper may help develop narrow-band (at the cooperative resonant frequency) and efficient on-chip lasers.

Another application of the cooperative effects discussed in this paper can be in implementing efficient quantum memories. As an example, erbium-doped crystals are being investigated as a memory platform for telecommunication photons compatible with the existing infrastructure. One limitation of Erbium and some other rare-earth ions is inefficient atomic spin preparation caused by the low branching ratio and their long

excited state lifetime. Optical cavities are being explored to mitigate this issue by inducing Purcell-enhanced emission and speeding up the preparation process [34]. The use of cavities, however, also reduces optical bandwidth for otherwise broadband rare-earth quantum memories. A low-bandwidth quantum memory can limit the efficiency or rate of communication. The enhanced cooperative emission of atomic arrays can provide alternative physics to better prepare atomic memories while using the entire bandwidth available by atoms. Moreover, the array engineering can in principle help with the fidelity of the memory as it can suppress the free-space scattering and therefore noise [35].

More specifically, let us consider the atomic frequency comb memory [36] that is being extensively used to realize broadband rare-earth solid-state quantum memories [4, 37–39]. The key to storage is the creation of equally spaced atomic absorption lines (i.e. atomic frequency comb) within the inhomogeneously broadened atomic transition. This is typically achieved by burning equally spaced spectral holes in a specific atomic transition, which then decays to an auxillary atomic state creating a comb-like structure of spectral antiholes. If the decay rate from the excited state is comparable to population decay rate between the ground-state levels, as is the case for Er-dopped crystals above 1 K temperature, efficient preparation of the atomic frequency comb can not be achieved. In the case of Er crystals, this constraint can be lifted using few-Tesla-large magnetic field and milli-Kelvin temperatures [40, 41]. For an array of atoms placed inside a resonator with linewidth much larger than the desired memory bandwidth and smaller than the inhomogeneous broadening width, the superadiance may be achieved for all comb lines enhancing the preparation efficiency.

In conclusion, we have provided a theory of light-atom interaction for an array of inhomogeneously broadened atoms inside optical resonators. We have discussed the regimes where cooperative and long-range atom-atom interactions can lead to enhanced light-atom coupling. We have proposed some applications of on-chip cooperative effects in both classical and quantum photonics.

Data availability statement

All data that support the findings of this study are included within the article (and any supplementary files).

Acknowledgment

The authors would like to thank Francis Robicheaux for stimulating discussions and theory guidance. The authors acknowledge funding from National Science Foundation Career Award Number: 2144 356. The work is also partly supported by the U.S. Department of Energy, Office of Science, Office of Advanced Scientific Computing Research, through the Quantum Internet to Accelerate Scientific Discovery Program under Field Work Proposal 3ERKJ381.

ORCID iD

Trevor Kling https://orcid.org/0000-0003-1496-7717

References

- [1] Bhaskar M K et al 2020 Experimental demonstration of memory-enhanced quantum communication Nature 580 60-64
- [2] Lago-Rivera D, Grandi S, Rakonjac J V, Seri A and de Riedmatten H 2021 Telecom-heralded entanglement between multimode solid-state quantum memories *Nature* 594 37–40
- [3] Kimble H J 1998 Strong interactions of single atoms and photons in cavity qed Phys. Scr. 1998 127
- [4] Ortu A Rakonjac J V, Holzäpfel A, Seri A, Grandi S, Mazzera M, de Riedmatten H and Afzelius M 2022 Multimode capacity of atomic-frequency comb quantum memories Quantum Sci. Technol. 7 035024
- [5] Masson S J and Asenjo-Garcia A 2022 Universality of dicke superradiance in arrays of quantum emitters Nat. Commun. 13 1-7
- [6] Lukin D M et al 2022 Optical superradiance of a pair of color centers in an integrated silicon-carbide-on-insulator microresonator (arXiv:2202.04845)
- [7] Goban A Hung C-L, Hood J, Yu S-P, Muniz J, Painter O and Kimble H 2015 Superradiance for atoms trapped along a photonic crystal waveguide Phys. Rev. Lett. 115 063601
- [8] Ma Y, Ma Y-Z, Zhou Z-Q, Li C-F and Guo G-C 2021 One-hour coherent optical storage in an atomic frequency comb memory Nat. Commun. 12 2381
- [9] Raha M et al 2020 Optical quantum nondemolition measurement of a single rare earth ion qubit Nat. Commun. 11 1605
- [10] Kindem J M Ruskuc A, Bartholomew J G, Rochman J, Huan Y Q and Faraon A 2020 Control and single-shot readout of an ion embedded in a nanophotonic cavity Nature 580 201–4
- [11] Nandi A Jiang X, Pak D, Perry D, Han K, Bielejec E S, Xuan Y and Hosseini M 2020 Controlling light emission by engineering atomic geometries in silicon photonics *Opt. Lett.* 45 1631–4
- [12] Chang T-H, Fields B M, Kim M E and Hung C-L 2019 Microring resonators on a suspended membrane circuit for atom–light interactions *Optica* 6 1203–10
- [13] Pak D et al 2022 Long-range cooperative resonances in rare-earth ion arrays inside photonic resonators Commun. Phys. 5 89

- [14] Nandi A, An H and Hosseini M 2021 Coherent atomic mirror formed by randomly distributed ions inside a crystal Opt. Lett. 46 1880–3
- [15] Gao R Yao N, Guan J, Deng Li, Lin J, Wang M, Qiao L, Fang W and Cheng Y 2022 Lithium niobate microring with ultra-high Q factor above 10⁸ Chin. Opt. Lett. 20 011902
- [16] Thiel C W, Sun Y, Böttger T, Babbitt W R and Cone R L 2010 Optical decoherence and persistent spectral hole burning in Tm3+:Linbo3 J. Lumin. 130 1598–602
- [17] Douglas J S Habibian H, Hung C-L, Gorshkov A V, Kimble H J and Chang D E 2015 Quantum many-body models with cold atoms coupled to photonic crystals Nat. Photon. 9 326–31
- [18] Kurizki G 1990 Two-atom resonant radiative coupling in photonic band structures Phys. Rev. A 42 2915
- [19] Mirhosseini M Kim E, Zhang X, Sipahigil A, Dieterle P B, Keller A J, Asenjo-Garcia A, Chang D E and Painter O 2019 Cavity quantum electrodynamics with atom-like mirrors Nature 569 692–7
- [20] Furuya K, Nandi A and Hosseini M 2020 Study of atomic geometry and its effect on photon generation and storage (invited) Opt. Mater. Express 10 577–87
- [21] Chang D E, Sørensen A S, Demler E A and Lukin M D 2007 A single-photon transistor using nanoscale surface plasmons *Nat. Phys.* 3 807–12
- [22] Solano P, Barberis-Blostein P, Fatemi F K, Orozco L A and Rolston S L 2017 Super-radiance reveals infinite-range dipole interactions through a nanofiber Nat. Commun. 8 1857
- [23] Masson S J, Ferrier-Barbut I, Orozco L A, Browaeys A and Asenjo-Garcia A 2020 Many-body signatures of collective decay in atomic chains Phys. Rev. Lett. 125 263601
- [24] Robicheaux F 2021 Theoretical study of early-time superradiance for atom clouds and arrays Phys. Rev. A 104 063706
- [25] Srinivasan K and Painter O 2007 Mode coupling and cavity—quantum-dot interactions in a fiber-coupled microdisk cavity Phys. Rev. A 75 023814
- [26] Tanji-Suzuki H et al 2011 Chapter 4—interaction between atomic ensembles and optical resonators: classical description Advances in Atomic, Molecular and Optical Physics vol 60, ed E Arimondo, P Berman and C Lin (New York: Academic) pp 201–37
- [27] Hood J D Goban A, Asenjo-Garcia A, Lu M, Yu S-P, Chang D E and Kimble H J 2016 Atom–atom interactions around the band edge of a photonic crystal waveguide *Proc. Natl Acad. Sci.* 113 10507–12
- [28] Asenjo-Garcia A, Hood J, Chang D and Kimble H 2017 Atom-light interactions in quasi-one-dimensional nanostructures: a green's-function perspective *Phys. Rev.* A **95** 033818
- [29] Bradac C Johnsson M T, Breugel M V, Baragiola B Q, Martin R, Juan M L, Brennen G K and Volz T 2017 Room-temperature spontaneous superradiance from single diamond nanocrystals Nat. Commun. 8 1205
- [30] Scheibner M Schmidt T, Worschech L, Forchel A, Bacher G, Passow T and Hommel D 2007 Superradiance of quantum dots Nat. Phys. 3 106
- [31] Shahbazyan T V, Raikh M E and Vardeny Z V 2000 Mesoscopic cooperative emission from a disordered system Phys. Rev. B 61 13266–76
- [32] Norcia M A and Thompson J K 2016 Cold-strontium laser in the superradiant crossover regime Phys. Rev. X 6 011025
- [33] Luo Q et al 2022 On-chip ytterbium-doped lithium niobate microdisk lasers with high conversion efficiency Opt. Lett. 47 854–7
- [34] Dibos A, Raha M, Phenicie C and Thompson J D 2018 Atomic source of single photons in the telecom band Phys. Rev. Lett. 120 243601
- [35] Asenjo-Garcia A, Moreno-Cardoner M, Albrecht A, Kimble H and Chang D E 2017 Exponential improvement in photon storage fidelities using subradiance and 'selective radiance' in atomic arrays Phys. Rev. X 7 031024
- [36] Afzelius M, Simon C, De Riedmatten H and Gisin N 2009 Multimode quantum memory based on atomic frequency combs *Phys. Rev.* A **79** 052329
- [37] Yang T-S et al 2018 Multiplexed storage and real-time manipulation based on a multiple degree-of-freedom quantum memory Nat. Commun. 9 3407
- [38] Laplane C Jobez P, Etesse J, Timoney N, Gisin N and Afzelius M 2015 Multiplexed on-demand storage of polarization qubits in a crystal New J. Phys. 18 013006
- [39] Ortu A, Holzäpfel A, Etesse J and Afzelius M 2022 Storage of photonic time-bin qubits for up to 20 ms in a rare-earth doped crystal npi Quantum Inf. 8 29
- [40] Rančić M, Hedges M P, Ahlefeldt R L and Sellars M J 2018 Coherence time of over a second in a telecom-compatible quantum memory storage material Nat. Phys. 14 50–54
- [41] Jiang M-H et al 2022 Quantum storage of entangled photons at telecom wavelengths in a crystal (arXiv:2212.12898)